Detection of Sub-Shot-Noise Spatial Correlation in High-Gain Parametric Down Conversion

O. Jedrkiewicz,[1] Y.-K Jiang,[2] E. Brambilla,[1] A. Gatti,[1] M. Bache,[1] L. A. Lugiato,[1] and P. Di Trapani[1]
[1]*INFM, Dipartimento di Fisica e Matematica, Universita' dell'Insubria, Via Valleggio 11, 22100 Como, Italy*
[2]*Department of Electronic Science and Applied Physics, Fuzhou University, 350002 Fuzhou, China*
(Received 26 July 2004; published 6 December 2004)

Using a 1 GW, 1 ps pump laser pulse in high-gain parametric down conversion allows us to detect sub-shot-noise spatial quantum correlation with up to 100 photoelectrons per mode by means of a high efficiency charge coupled device. The statistics is performed in single shot over independent spatial replica of the system. Evident quantum correlations were observed between symmetrical signal and idler spatial areas in the far field. In accordance with the predictions of numerical calculations, the observed transition from the quantum to the classical regime is interpreted as a consequence of the narrowing of the down-converted beams in the very high-gain regime.

DOI: 10.1103/PhysRevLett.93.243601 PACS numbers: 42.50.Dv, 42.50.Ar, 42.65.Lm

Spatial quantum optical fluctuations are studied because of new potential applications of quantum optical procedures in parallel processing and multichannel operation. Examples are quantum holography [1], the quantum teleportation of optical images [2], and the measurements of small displacements beyond the Rayleigh limit [3]. The process of parametric down conversion (PDC) is particularly suitable for the study of spatial effects because of its large emission bandwidth in the spatial frequency domain [4]. There is now a large body of literature on spatial effect in the low-gain regime, where photon pairs are detected via coincidence counting [5]. Nevertheless, to date, spatial correlation measurements in this regime have not evidenced any relevant quantum effect [6,7]. On the other side, measurements performed in the medium-gain regime (pump power ≤ 1 MW) evidenced the twin-beam character of the PDC emission [8], i.e., a sub-shot-noise correlation between the photon numbers of the whole signal and idler beams. Recent theoretical investigations done for an arbitrary gain [9,10] have predicted multimode spatial correlations below shot noise between several portions of the signal and idler emission cones that correspond to phase-conjugate modes. There is a minimum size of the modes that have to be detected in order to observe a quantum correlation, which we shall refer to as the *coherence area*. This is determined by the conditional uncertainty in the directions of propagation of the twin photons, and is roughly given by the inverse of the near-field gain area [9].

Here we report on the first quantum spatial measurements of PDC radiation performed by using a low-repetition rate (2 Hz) pulsed high-power laser (1 GW, 1 ps). This enables us to tune the PDC to the high-gain regime while keeping a large pump-beam size ($\sim$1 mm). The huge number of transverse modes [roughly given by the ratio between (i) the angular bandwidth of the PDC and (ii) the inverse of the near-field gain area] allows us to concentrate on a portion of the parametric fluorescence close to the collinear direction and within a narrow frequency bandwidth around degeneracy. This portion still contains a large (> 1000) number of pairs of signal or idler correlated phase-conjugate modes, propagating at symmetrical directions with respect to the pump in order to fulfill the phase-matching constraints. In the far field, where the measurement is performed, the couples of modes correspond to pairs of symmetrical spots, which can be considered as independent and equivalent spatial replica of the same quantum system. Thanks to the very large number of these, the statistical ensemble averaging necessary for the quantum measurement can be solely done over the *spatial* replicas *for each single pump-laser pulse*. This is in contrast with the experiment of [8] where the statistics was performed over different temporal replica of the system. The single-shot measurements reveal sub-shot-noise spatial correlations for a PDC gain corresponding to the detection of up to $\simeq 100$ photoelectrons per mode. Using a bandpass optical parametric amplifier, Ref. [11] measured the correlation between signal or idler

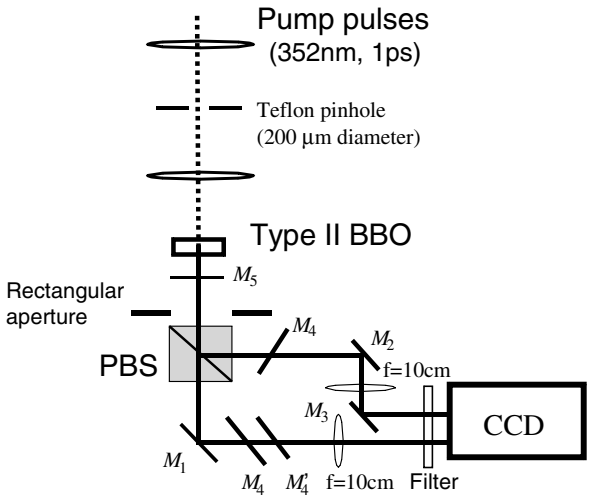

FIG. 1. Scheme of the experimental setup used for the spatial correlation measurements (see text).

phase-conjugate spatial modes and observed a transition from the quantum to the classical regime with increasing gain, but was unable to explain its origin. In our experiment we observe a similar transition and we are able to attribute it to a narrowing of the near-field gain profile that occurs at very high gain in presence of a bell-shaped pump beam, implying a broadening of the far-field coherence area. This was discovered by numerically solving the coupled three-wave equations in the framework of a 3D + 1 quantum model.

The experimental setup is sketched in Fig. 1. The third harmonic (352 nm) of a 1 ps, chirped-pulse amplified Nd:glass laser (TWINKLE, Light Conversion Ltd.) is used to pump a type II $5 \times 7 \times 4$ mm^3 beta-barium-borate (BBO) nonlinear crystal, operated in the regime of parametric amplification of the vacuum-state fluctuations. The input and output facets of the crystal are antireflection coated at 352 nm and 704 nm, respectively. The pump beam is spatially filtered and collimated to a beam waist of approximately 1 mm (FWHM) at the crystal input facet. The energy of the 352 nm pump pulse can be continuously tuned in the range 0.1–0.4 mJ by means of suitable attenuating filters and by changing the energy of the 1055 nm pump-laser pulse, allowing to have a gain G (intensity amplification factor) in the range $10 \leq G \leq 10^3$. The parametric fluorescence of the horizontally polarized signal and vertically polarized idler modes is emitted over two cones, whose apertures depend on the specific wavelengths (see, e.g., [12,13]). The BBO crystal ($\theta = 49.05°$, $\phi = 0$) is oriented in order to generate signal and idler radiation cones tangent to the collinear direction at the degenerate wavelength $\omega_s = \omega_i = \omega_p/2$ (s, i, and p referring to signal, idler, and pump, respectively). The fluorescence around the collinear direction is selected by a 5 mm $\times$ 8 mm aperture placed 15 cm from the output facet of the BBO, and is then transmitted through a polarizing beam splitter (PBS), which separates the signal and idler beams. The aperture prevents beam clipping by the PBS and thereby reduces substantially scattered radiation. The beams are finally sent onto two separate regions of a deep-depletion back illuminated charged coupled device (CCD) camera [14] (with quantum efficiency $\eta \approx 89\%$ at 704 nm), placed in the common focal plane of the two lenses ($f = 10$ cm) used to image the signal and idler far fields. The detection array has 1340×400 pixels, with a pixel size of 20 μm $\times$ 20 μm. Prior to the experiment, the CCD was calibrated with a coherent source allowing the retrieval of spatial shot-noise statistics in its full dynamic range [15]. In contrast to the case of photon-counting experiments (coincidence measurements), in our setup the correlation measurements are performed without using any narrowband interferential filters (IFs), since IFs unavoidably introduce relevant transmission losses reducing the visibility of sub-shot-noise correlations. The pump-frequency contribution is removed by using normal incidence (M_5) and at 45° (M_4) high-reflectivity (HR) mirrors coated for 352 nm placed before and after the PBS, respectively, and a low-band-pass color filter (90% transmission around 704 nm) placed in front of the CCD. A further HR at 352 nm mirror (M_4') is placed in one of the two arms at a suitable angle in order to balance the unequal transmission of the PBS in the two arms. All the optical components (except the color filter) have antireflection coatings at 704 nm. The estimated quantum efficiency of each detection line, which accounts for both the transmission losses and the detector efficiency, is $\eta_{\text{tot}} \simeq 75\%$.

Figure 2(a) shows a typical far-field image recorded in a single shot, where a fairly broadband radiation (i.e., the one transmitted by the rectangular aperture) is acquired in the signal (left) and idler (right) branches. The selection of the desired temporal and angular bandwidth around degeneracy is made by temporarily inserting in front of the CCD a 10 nm wide IF around 704 nm, allowing us to locate the collinear degeneracy point [see Fig. 2(b)]. The data analysis is limited within two rectangular boxes [black frames in Fig. 2(a)] corresponding to an angular bandwidth of 20 mrad $\times$ 8 mrad and to a temporal bandwidth smaller than 10 nm. The selected regions contain 4000 pixels each. In this work we investigate *pixel-pair* correlation, and since the size of the CCD pixel approximately corresponds to the physical size of a replica (coherence area), the ensemble is large enough to perform the desired statistics. A zoom of the

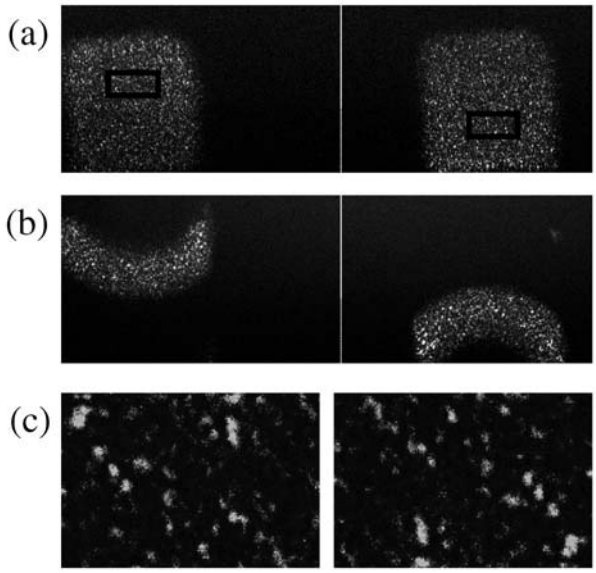

FIG. 2. (a) Single-shot far-field image recorded by the CCD for a pump-beam waist $w_0 \simeq 1$ mm and pump energy $\varepsilon_p \simeq 0.3$ mJ. The spatial areas for statistics are delimited by the black boxes selected within the degenerate signal and idler modes, spatially localized from the single-shot image recorded with the 10 nm-broad IF (b). (c) Zoom of two symmetrical areas of the signal and idler far fields.

selected areas is presented in Fig. 2(c), where the rather spectacular symmetry of the intensity distribution in the signal and idler branches shows the twin-beam character of the phase-conjugate modes.

The symmetrical pixel-pair correlation is evaluated experimentally by measuring the variance σ^2_{s-i} of the PDC photoelectrons (PE) difference $n_s - n_i$ of the signal or idler pixel pair versus the mean total number of down-converted PE of the pixel pair. This variance is $\sigma^2_{s-i} = \langle (n_s - n_i)^2 \rangle - \langle n_s - n_i \rangle^2$ where the averages are spatial averages performed over all the symmetrical pixel pairs contained in the chosen regions. Each single shot of the laser provides a different ensemble, characterized by its pixel-pair average PE number $\langle n_s + n_i \rangle$, in turn related to the parametric gain. In the experiment, ensembles corresponding to different gains are obtained by varying the pump-pulse energy. We note that the readout noise of the detector, its dark current, and some unavoidable light scattered from the pump, signal, and idler fields contribute with a non-negligible background noise to the process. This is taken into account by applying a standard correction procedure (see, for example, [16]), by subtracting the background fluctuations σ^2_b from the *effectively measured* variance $\sigma^2_{(s+b)-(i+b)}$ of the total intensity difference (signal + background) − (idler + background) obtaining $\sigma^2_{s-i} = \sigma^2_{(s+b)-(i+b)} - 2\sigma^2_b$. This background noise, having a standard deviation of seven counts (± 0.1 from shot to shot, estimated by repeating the measurement with the same pump-pulse energy) is measured in presence of pulse illumination over an area of the same size of the acquisition area and suitably displaced from the directly illuminated region. The validity of the data correction procedure and the shot-noise level calibration are made by sending in the setup (with no crystal) through the PBS a coherent circularly polarized pulsed beam (at 704 nm), and verifying for different laser energies that the intensity difference fluctuations from the two coherent portions of beams recorded on the CCD lie at the shot-noise level.

Figure 3 shows the experimental results where each point is associated with a different laser shot. The data are normalized to the shot-noise level (SNL), and their statistical spread accounts for the background correction. Although the noise on the individual signal and idler beams is found to be very high and much greater than their SNL ($= \langle n_s \rangle$ and $\langle n_i \rangle$, respectively), we observe an evident sub-shot-noise pixel-pair correlation up to gains characterized by $\langle n_s + n_i \rangle \approx 15$–18. Since in that regime the observed transverse size of the coherence areas (i.e., of the modes) is about 2–4 pixels, this approximately corresponds to 100 PE per mode. We can have an idea of the transverse size of the mode by looking at the standard two-dimensional cross-correlation degree $\gamma = (\langle n_s n_i \rangle - \langle n_s \rangle \langle n_i \rangle) / \sqrt{\sigma^2_s \sigma^2_i}$, between all the angularly symmetrical signal and idler pixels contained within the black boxes

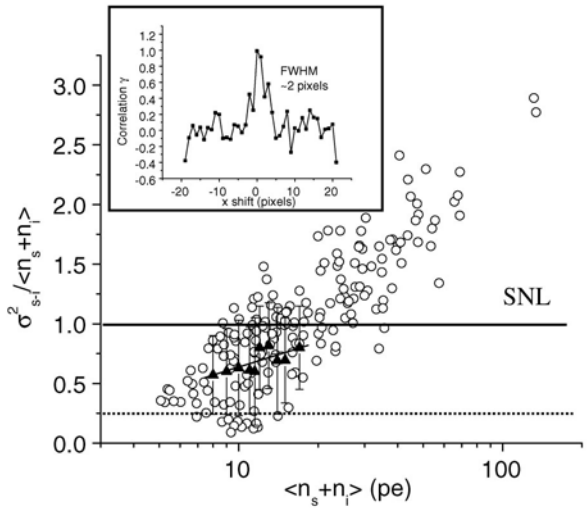

FIG. 3. Intensity difference variance σ^2_{s-i} normalized to the SNL $\langle n_s + n_i \rangle$. Each point (white circle) corresponds to a single-shot measurement where the spatial ensemble statistics has been performed over a 100×40 pixels region. The triangles (each one obtained by averaging the experimental points corresponding to a certain gain) and their linear fit illustrate the trend of the data in the region between $\langle n_s + n_i \rangle = 8$ and 20. Inset: typical correlation degree profile in the regime where $\langle n_s + n_i \rangle \simeq 8$ (see text).

[see Fig. 2(a)]. This can be plotted, for instance, as a function of the horizontal and vertical shifts of the recorded image on the CCD, keeping fixed the position of the boxes. In general, $|\gamma| \leq 1$ with $\gamma = 1$ for perfect correlation. A transverse section of the correlation function obtained from a single-shot image characterized by $\langle n_s + n_i \rangle \approx 8$ is plotted in the inset of Fig. 3 as a function of the horizontal shift x (in pixel units), revealing a transverse mode size of about two pixels. As expected, virtually perfect correlation (in our case, the peak value is $\simeq 0.99$) is obtained for perfect determination (i.e., within one pixel) of the center of symmetry between the signal and the idler regions.

In order to interpret the observed transition from quantum to classical regime we present in Fig. 4 the results of the numerical calculations. The full quantum model accounts for the two transverse and the temporal degrees of freedom with propagation along the crystal, for the angular and chromatic material dispersion up to the second order, for the finite spatial and temporal widths of the Gaussian pump pulse, and for the experimental quantum efficiency η_{tot} (see [9] for more details). The crystal and input-pulse parameters are those relative to the experiment. The figure presents σ^2_{s-i}, normalized to the SNL, versus the size of the detection area for different gains. Each point is the result of a statistics performed over one single laser shot. The case $N = 1$ corresponds to the experiment. The simulations (data not shown) outline that, in spite of the fixed pump-beam diameter, the signal

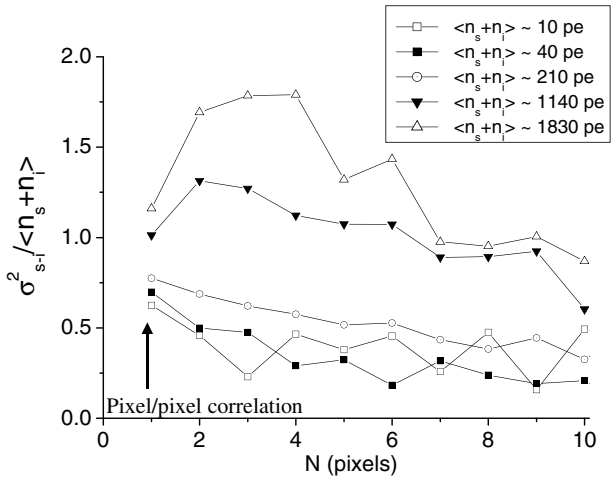

FIG. 4. Numerical calculation of σ^2_{s-i} (normalized to SNL) between symmetrical portions of signal and idler plotted as a function of the detection area represented by $N \times N$ binned pixels. Different curves correspond to different values of the gain characterized by the mean number of down-converted PE per pixel pair $\langle n_s + n_i \rangle$.

and idler beam diameters at the crystal output strongly depend on the gain and decrease when the latter increases. This can be easily interpreted when considering that the signal and idler beam size maps not the pump-beam profile but the actual parametric amplification gain profile $G(\mathbf{r}) \sim \cosh^2[\sigma A(\mathbf{r})L]$ [17] (L being the crystal length, A the pump field amplitude, and σ a parameter proportional to the setting characteristics), as long as filtering due to the limited spatial bandwidth does not take place [18]. On narrowing the size of the PDC beams, the coherence areas in the far field (i.e., the modes) increase their size, as straightforward consequence of the convolution theorem in Fourier analysis [12]. Since revealing quantum correlations requires detection areas larger (or comparable) to the mode size (as also discussed in [9]), it is necessary when increasing the gain to have larger detectors in order to obtain sub-shot-noise variance as shown in Fig. 4. Note that Fig. 4 evidences the transition from quantum to classical regime in case of single-pixel detection ($N = 1$) for a gain that is higher than in the experiment. Indeed, in the experiment, excess noise is observed for $\langle n_s + n_i \rangle > 20$, which we attribute first to the effect of residual scattered light whose contribution grows linearly with the radiation fluence and is thus expected to overcome the shot noise at large pumping, and second to the uncertainty in the determination of the symmetry center of the signal and idler image portions. In fact, simulations have shown that an uncertainty as small as a few microns (i.e., a fraction of the pixel size, unavoidable experimentally), prevents to observe sub-shot-noise correlation as soon as $\langle n_s + n_i \rangle$ exceeds some tens of PE, while still preserving sub-shot-noise correlation for smaller gain values. Finally, the maximum level of noise reduction observed experimentally agrees with the theoretical limit (dotted line in Fig. 3) determined by the total losses of the system ($\sim 1 - \eta_{\text{tot}}$ [9]).

In conclusion, we have shown that twin beams of light generated in PDC exhibit sub-shot-noise spatial correlation by measuring in the far field an evident quantum noise reduction on the signal or idler intensity difference. A transition to above shot-noise correlation is observed as the gain increases. This quantum-to-classical transition, in agreement with numerical simulations, is explained as a narrowing of the signal or idler beams with increased gain. This leads in turn to a larger far-field mode size and therefore also to the need of larger pixels to observe sub-shot-noise correlation [9]. This will be the aim of a future work. To our knowledge, this is the first experimental investigation of quantum spatial correlations in the high-gain regime, where the huge number of transverse spatial modes is detected in single shot by means of a high-quantum-efficiency CCD.

This work was supported by projects FET QUANTIM, PRIN of MIUR, FIRB01, INTAS 2001-2097. M. B. acknowledges support from the Carlsberg Foundation.

[1] A. F. Abouraddy, B. E. A. Saleh, A. V. Sergienko, and M. C. Teich, Opt. Express **9**, 498 (2001).
[2] I. V. Sokolov, M. I. Kolobov, A. Gatti, and L. A. Lugiato, Opt. Commun. **193**, 175 (2001).
[3] N. Treps *et al.*, Phys. Rev. Lett. **88**, 203601 (2002).
[4] F. Devaux and E. Lantz, Eur. Phys. J. D **8**, 117 (2000).
[5] L. A. Lugiato, A. Gatti, and E. Brambilla, J. Opt. B **4**, S176 (2002), and references therein.
[6] B. M. Jost *et al.*, Opt. Express **81**, 3 (1998).
[7] S. S. R. Oemrawsingh, W. J. van Drunen, E. R. Eliel, and J. P. Woerdman, J. Opt. Soc. Am. B **19**, 2391 (2002).
[8] O. Aytur and P. Kumar, Phys. Rev. Lett. **65**, 1551 (1990).
[9] E. Brambilla, A. Gatti, M. Bache, and L. A. Lugiato, Phys. Rev. A **69**, 023802 (2004).
[10] A. Gatti, E. Brambilla, L. A. Lugiato, and M. I. Kolobov, Phys. Rev. Lett. **83**, 1763 (1999); Eur. Phys. J. D **15**, 117 (2001).
[11] M. L. Marable, S.-K. Choi, and P. Kumar, Opt. Express **2**, 84 (1998).
[12] A. Berzanskis *et al.*, Phys. Rev. A **60**, 1626 (1999).
[13] M. H. Rubin, Phys. Rev. A **54**, 5349 (1996).
[14] J. R. Janesick, *Scientific Charge-Coupled Devices* (SPIE Press Bellingham, Washington, 2001), pp. 204–205; see also Roper Scientific GMBH, http://www.roperscientific.de/theory.html.
[15] Y.-K. Jiang *et al.*, Eur. Phys. J. D **22**, 521 (2003).
[16] A. Mosset, F. Devaux, G. Fanjoux, and E. Lantz, Eur. Phys. J. D **28**, 447 (2004).
[17] S. A. Akhmanov, V. A. Vysloukh, and A. S. Chirkin, *Optics of Femtosecond Laser Pulses* (American Institute of Physics, New York, 1992), p. 151.
[18] P. Di Trapani, G. Valiulis, W. Chinaglia, and A. Andreoni, Phys. Rev. Lett. **80**, 265 (1998).